Neuroendocrinology Letters Volume 46 No. 6 2025
ISSN: 0172-780X; ISSN-L: 0172-780X; Electronic/Online ISSN: 2354-4716
Web of Knowledge / Web of Science: Neuroendocrinol Lett
Pub Med / Medline: Neuro Endocrinol Lett

ORIGINAL PAPER

MRA morphologic study of the vertebrobasilar artery system in patients with primary hemifacial spasm

Hao Zhang[1], Jinming Yan[1]

1 Department of Imaging, Xuzhou Hospital of Traditional Chinese Medicine, Xuzhou, Jiangsu 221000, China.

Correspondence to: Jinming Yan, Department of Imaging, Xuzhou Hospital of Traditional Chinese Medicine, 169 South Zhongshan Road, Xuzhou, Jiangsu 221000, China
tel.: +86-0516-68692044; e-mail: yanjinming528@163.com

Submitted: 2025-08-28 Accepted: 2025-12-02 Published online: 2025-12-15

Key words: **Primary hemifacial spasm; Vertebrobasilar artery; Magnetic resonance angiography; Morphologic abnormalities; Neurology**

Neuroendocrinol Lett 2025; **46**(6):356–365 **PMID:** 41420884 46062502

Abstract

PURPOSE: This study assessed the efficacy of 3.0T magnetic resonance angiography (MRA) in individuals with primary hemifacial spasm (pHFS) by investigating the relationship between alterations in the morphology of the vertebrobasilar artery system and pHFS.

METHODS: A comparison was made between pHFS patients and healthy controls with respect to vertebral artery diameter, displacement rate, and other relevant parameters to explore the potential role of morphologic abnormalities in the vertebrobasilar arteries in the pathogenesis of pHFS. Independent t-tests and Wilcoxon rank-sum tests were used with statistical significance set at a $p < 0.05$.

RESULTS: A total of 100 pHFS patients and 150 healthy participants underwent 3.0T MRA scans for this analysis. The right vertebral artery (VA) diameter in the pHFS group was larger than the healthy control (HC) group (2.71 mm vs. 2.47 mm; $p < 0.05$) and the left VA deviation distance in the pHFS group was greater than the HC group (7.99 mm vs. 5.27 mm; $p < 0.05$). The basilar artery deviation distance in the pHFS group was greater than the HC group (7.41 mm vs. 4.78 mm; $p < 0.05$). The VA deviation rates in the pHFS group were significantly higher than the HC group (89% vs. 72% and 96% vs. 84.67%, respectively; $p < 0.05$). The VA scores on the symptomatic and non-symptomatic sides were significantly different ($p < 0.05$). VA migration increased with age ($p = 0.034$, $r = 0.225$).

CONCLUSION: The results imply a potential association between morphologic irregularities in the vertebrobasilar arteries and pHFS. Limitations of the study included substantial missing data for displacement measurements (64%–67%), age differences between groups, and selection bias from the surgical population.

INTRODUCTION

Hemifacial spasm (HFS) is a condition characterized by involuntary contractions on one side of the face, typically starting around the eye muscles and progressing to the muscles around the nose, mouth, cheeks, and neck (Aktan & Depierreux, 2024). Epidemiologic data have revealed an HFS incidence rate of 7–15 per 100,000 individuals (Nurminen *et al.* 2023; Truong *et al.* 2024; Wang *et al.* 2024). The prognosis for HFS may be impacted by concurrent psychologic conditions, such as stress and anxiety (Wang *et al.* 2014; Wang *et al.* 2024). Although HFS typically presents in adults, HFS is generally non-heritable, except for rare familial cases.

Compression of blood vessels at the root exit zone (REZ) of the facial nerve is the leading cause of primary HFS (pHFS), while secondary HFS (sHFS) can arise from conditions, such as facial palsies, cerebellopontine angle tumors, and Chiari I malformations. The incidence of pHFS is 3–4-fold greater than sHFS (Colosimo *et al.* 2006; Fang *et al.* 2022). Key vessels that compress the REZ include the anterior inferior cerebellar artery (AICA), posterior inferior cerebellar artery (PICA), and vertebral artery [VA] (Błaszczyk *et al.* 2024). Various compression patterns between vessels and the facial nerve have been reported, encompassing circular, arachnoidal, perforating, branching, sandwich, and tandem patterns (Campos-Benitez & Kaufmann, 2008; Joo, 2023).

The diagnosis of HFS is primarily based on clinical history and physical examination. Distinctive characteristics of HFS involve unilateral, irregular, tonic, or clonic contractions of facial muscles. The presence of the "other Babinski sign," which manifests as automatic elevation of the eyebrows upon eye closure, contributes significantly to diagnosing HFS with a specificity of 100% and a sensitivity of 86% (Nurminen *et al.* 2023; Aktan & Depierreux, 2024; Truong *et al.* 2024; Wang *et al.* 2024). Furthermore, magnetic resonance angiography (MRA), magnetic resonance imaging (MRI), and computer tomography (CT) have crucial roles in confirming the diagnosis of HFS (Perren & Magistris, 2014; Dou *et al.* 2016; Zhou *et al.* 2022; Hou *et al.* 2024; Duvvuri *et al.* 2025). MRA enhances the visualization of small vessels through high-resolution imaging and accurately delineates the spatial relationship between the facial nerve and the compressing vessel by aligning scans with the course of the nerve (Hou *et al.* 2024).

Previous studies, including an investigation of anatomic VA deviations in HFS by our group (Yan *et al.* 2021), have established morphologic associations. However, quantitative characterization using standardized 3.0T MRA protocols in surgical populations is limited, which was the motivation for the current investigation. The relationship between anatomic variations in the basilar artery (BA) system and the development of pHFS requires further research.

Therefore, this study investigated the link between BA morphologic abnormalities and pHFS symptoms. Moreover, the diagnostic capability of 3.0 T MRA in identifying primary pHFS was determined.

MATERIALS AND METHODS

Research subjects

Retrospective ethical approval was obtained from the Ethics Committee of Xuzhou Hospital of Traditional Chinese Medicine (approval number: 2022-189) on 18 January 2022 for use of patient data collected between July 2018 and May 2020. Oral informed consent was obtained from each participant. This study retrospectively collected data from 100 patients diagnosed with pHFS who underwent microvascular decompression (MVD) in the Neurosurgery Department of Xuzhou

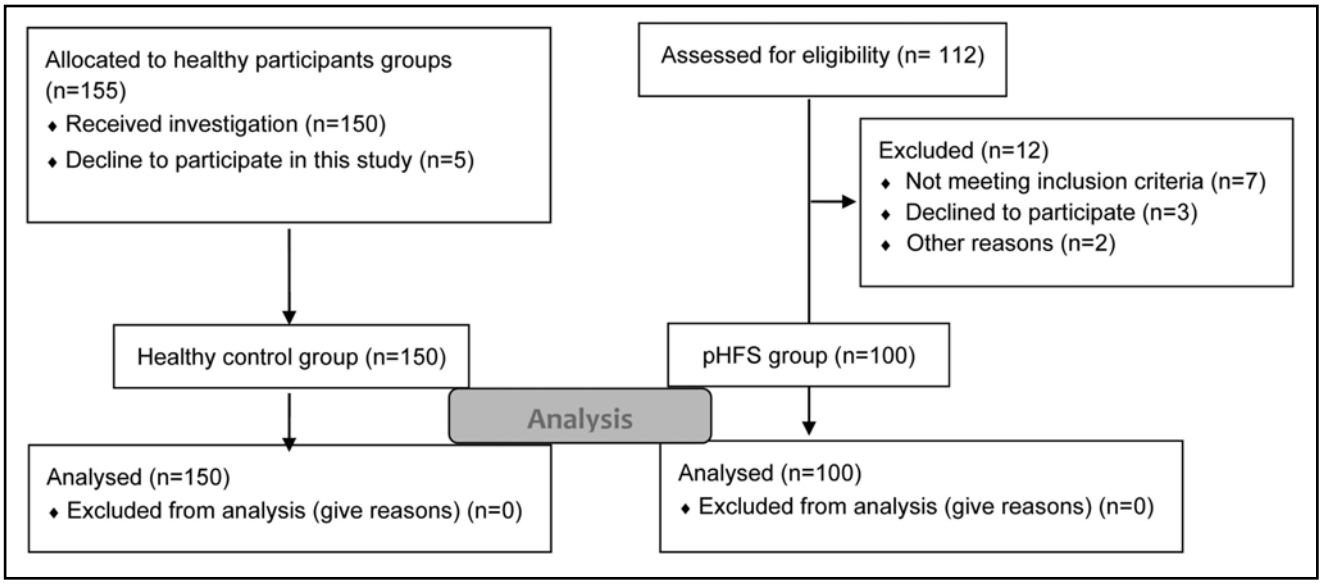

Fig. 1. Flowchart of the study participants.

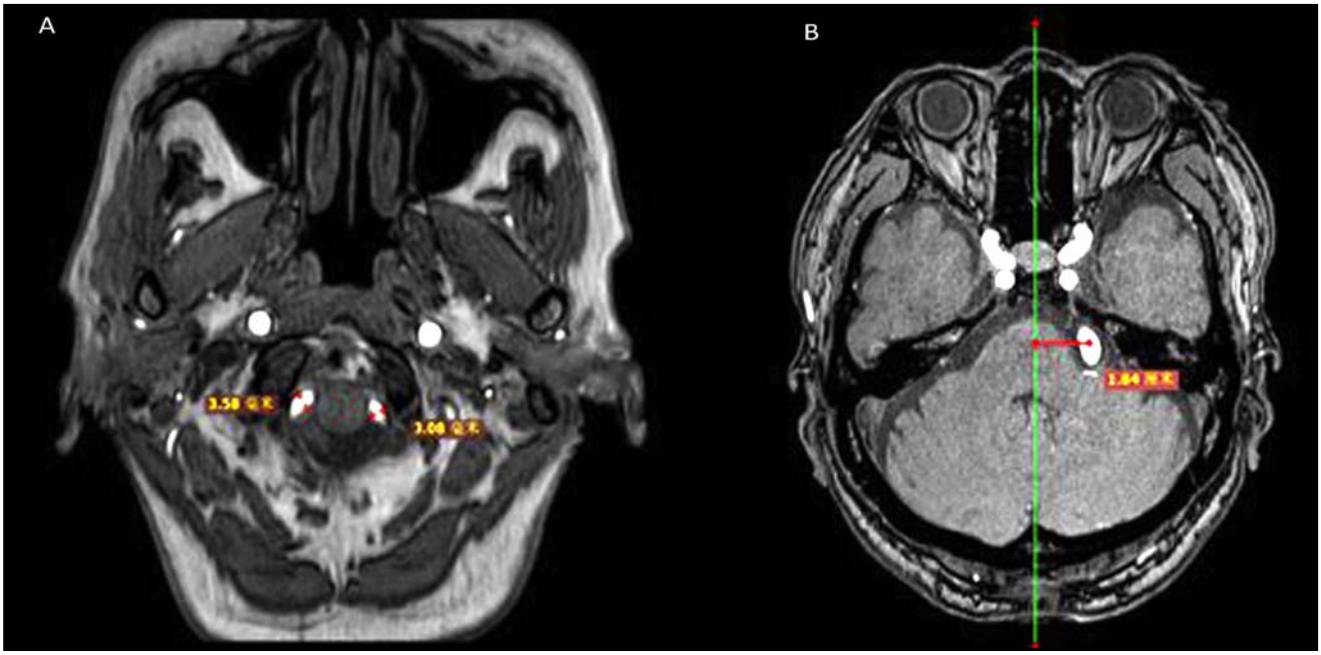

Fig. 2. Representative 3D time-of-flight magnetic resonance angiography (3D TOF MRA) images of the vertebrobasilar artery system. Images acquired on Philips Ingenia II 3.0T MR scanner using parameters: TR, 25 ms; TE, 1.71 ms; FOV, 160 × 160 × 45 mm; and matrix size, 200×200 with the scan range from the foramen magnum-to-the corpus callosum level.
A. Red arrow shows the measurement of the lumen diameters of the bilateral vertebral and basilar arteries in a perpendicular direction.
B. Red arrow shows the furthest blood vessel offset distance: the vertical distance from the vascular center at the maximum deviation of the blood vessel to the midline of the brain.

Hospital of Traditional Chinese Medicine between July 2018 and May 2020 (Figure 1). The control group (healthy control [HC]) was comprised of 150 healthy individuals undergoing routine health check-ups during the same period (Figure 1). There were 100 patients in the pHFS group with a male-to-female ratio of 1:2.03 consisting of 33 males (33%) and 67 females (67%) 31–85 years of age (mean age, 56.96 ± 9.61 years). The HC group included 150 individuals with a male-to-female ratio of 1:0.9 consisting of 79 males (52.67%) and 71 females (47.33%) 14–59 years of age (mean age, 49.36 ± 6.69 years).

The inclusion criteria for the pHFS group were as follows: 1) diagnosed with HFS undergoing MVD surgery; 2) preoperative MRA scan demonstrating an intact vertebrobasilar arterial (VBA) system; 3) absence of intracranial vascular malformations; and 4) absence of intracranial organic lesions. The exclusion criteria for the pHFS group included: 1) a history of prior cranial surgery; 2) patients with sHFS; and 3) inability to undergo MRA scan. The inclusion criteria for the HC group were as follows: 1) no history of intracranial diseases; and 2) MRI scan revealing clear MRA images with an intact VBA system. The exclusion criteria for the HC group included: 1) a history of cranial surgery; and 2) presence of definite cerebral vascular malformations or intracranial organic lesions on MRI.

Equipment

A Philips Ingenia II 3.0T MR scanner and the accompanying Nebula workstation incorporating a 16-channel head coil were used in the current study. MRA examinations were performed by an experienced radiologist with > 5 years of experience. The MRA data were validated by a senior radiologist with > 10 years of experience. The two radiologists were blinded to patient grouping when the MRA examinations were performed. Image analysis was performed by two experienced neuroradiologists with > 10 years of experience who were blinded to the clinical diagnosis.

Data acquisition

Data acquisition involved measuring vessel diameters and displacement distances on axial images of three-dimensional time-of-flight (3D TOF) MRA sequences. The 3D TOF MRA scan parameters were as follows: time resolved (TR), 25 ms; echo time (TE), 1.71 ms; field of view (FOV), 160 × 160 × 45 mm; and matrix size, 200×200 with the scan range from the foramen magnum-to-the corpus callosum level. The lumen diameters of the VAs and BA were measured at the upper, middle, and lower levels on both sides perpendicular to the blood vessel course. Vessel diameter was defined as the averaged diameter based on the measured data at the different levels (Figure 2A). The VA displacement distance on both sides was the maximum deviation from the midline. The displacement distance at the confluence of the VBAs was the maximum deviation from the midline to the confluence of the VBAs. The displacement distance of the BA was the sum of the offset distances on both sides of the BA crossing the midline. The measurement for the displacement

Tab. 1. Morphologic characteristics of the vertebrobasilar artery

Diameter/Displacement	HCs (n = 150)	Missing HC data	pHFS (n = 100)	Missing pHFS data	*p* value
Left vertebral artery diameter (mm)					0.1615
Number of cases (n/%)	150/100%	0/0%	99/99%	1/1.0%	
Mean ± standard deviation	2.88±0.65		3.01±0.81		
50% (25%, 75%)	2.83 (2.47, 3.27)		3.03 (2.45, 3.61)		
(Minimum, Maximum)	(1.32, 4.78)		(1.10, 5.08)		
Right vertebral artery diameter (mm)					0.0118
Number of cases (n/%)	150/150%	0/0%	100/100%	0/0%	
Mean ± standard deviation	2.47±0.61		2.71±0.82		
50% (25%, 75%)	2.44 (2.01, 2.91)		2.74 (2.08, 3.29)		
(Minimum, Maximum)	(1.30, 4.59)		(1.09, 5.28)		
Left vertebral artery displacement (mm)					0.0081
number of cases (n/%)	49/32.7%	101/67.3%	36/36.0%	64/64.0%	
Mean ± Standard Deviation	5.27±3.19		7.99±4.49		
50% (25%,75%)	4.22 (2.73, 6.91)		8.14 (3.76, 10.82)		
(Minimum, Maximum)	(1.45, 14.43)		(1.39, 17.00)		
Right vertebral artery displacement (mm)					0.0717
The number of cases (n/%)	59/39.3%	91/60.7%	53/53.0%	47/47.0%	
Mean ± standard deviation	4.98±2.77		6.41±4.20		
50% (25%, 75%)	4.55 (2.91, 6.18)		6.11 (3.06, 8.04)		
(Minimum, Maximum)	(1.09, 13.50)		(0.91, 19.10)		
Vertebrobasilar convergent displacement distance (mm)					0.1607
Number of cases (n/%)	107/71.3%	43/28.7%	85/85.0%	15/15.0%	
Mean ± standard deviation	4.72±2.57		5.92±4.14		
50% (25%, 75%)	4.22 (2.73, 6.18)		4.73 (2.74, 7.45)		
(Minimum, Maximum)	(1.09, 13.50)		(0.91, 19.30)		
Basilar artery diameter (mm)					0.2593
Number of cases (n/%)	149/99.3%	1/0.7%	99/99%	1/1.0%	
Mean ± standard deviation	3.31±0.50		3.27±0.74		
50% (25%, 75%)	3.32 (3.00, 3.68)		3.17 (2.83, 3.64)		
(Minimum, Maximum)	(2.01, 4.42)		(1.98, 6.90)		
Basilar artery displacement (mm)					0.0000
number of cases (n/%)	150/100%	0/0%	100/100%	0/0%	
Mean ± standard deviation	4.78±4.00		7.41±5.28		
50% (25%, 75%)	3.91 (1.71, 6.92)		6.19 (3.61, 9.57)		
(Minimum, Maximum)	(0.00, 16.72)		(0.00, 23.23)		

Tab. 2. Comparison of morphologic characteristics (offset rate) of the arterial

Morphologic characteristics		pHFS 100 cases	HCs 150 cases	c^2 value	*p* value
Left/right vertebral arteries	Displacement	89 (89.00)	108 (72.00)	10.380	0.001
	Non-displacement	11 (11.00)	42 (28.00)		
Basilar artery	Displacement	96 (96.00)	127(84.67)	8.000	0.005
	Non-displacement	4 (4.00)	23 (15.33)		
Convergence of the vertebral base	Left displacement	45 (45.00)	59 (39.86)	5.603	0.061
	Middle	15 (15.00)	41 (27.70)		
	Right displacement	40 (40.00)	48 (32.43)		

distance was made vertically from the vessel center at the point of maximum deviation to the brain midline (Figure 2B). Annotations were precise to 0.01 mm using the Philips workstation. VA displacements in patients with pHFS were assessed based on the VA scoring criteria according to Xi'an Jiaotong University Second Affiliated Hospital (Yan *et al.* 2021). The scoring was evaluated at the facial nerve level on axial images. If both VAs were on both sides of the midline, each side was scored 1 point each. If only one VA was at the midline, this side was scored 0.5 points and the other side was scored 1.5 points. If both VAs were on the same side of the midline, this side was scored 2 points and 0 points for the other side.

Statistical analysis

Statistical analysis was performed using SPSS 23.0. Descriptive statistics were utilized to present normally distributed data (age, VBA lumen diameter, and displacement distance) as the mean ± standard deviation, while non-normally distributed data are represented by the median (percentiles). Counts data for responsible vessels, dominant VA, and VA scores are detailed. Group comparisons for differences in VA lumen diameter were performed using an independent samples t-test, whereas disparities in BA lumen diameter, displacement distance, and VA displacement distance were assessed using the Wilcoxon rank-sum test. Group variations in dominant VA, responsible vessels, and VA scores were evaluated using a χ^2 test or Fisher's exact test. Correlation analysis between VBA lumen diameter and displacement distance was carried out using Pearson or Spearman correlation analysis depending on the normality of the data. A significance level of $p < 0.05$ was considered statistically significant.

RESULTS

General characteristics of subjects

The pHFS group included 100 individuals comprised of 33 males (33%) and 67 females (67%) with a male-to-female ratio of 1:2.03. The HC group consisted of 150 individuals with 79 males (52.67%) and 71 females (47.33%) and a male-to-female ratio of 1:0.9. The pHFS group was significantly older than the HC group (56.96 ± 9.61 years vs. 49.36 ± 6.69 years, respectively; $p < 0.001$), representing a potential confounding variable.

Morphologic characteristics of the VBA

Substantial differences were identified in the diameter of the right VA, left VA displacement, and BA displacement between the HC and pHFS groups. The pHFS group had a right VA diameter of 2.71 mm, which was larger than the 2.47 mm diameter in the HC group ($p < 0.05$). Furthermore, the left VA displacement in the pHFS group was 7.99 mm, which exceeded the displacement of 5.27 mm in the HC group ($p < 0.05$). Moreover, the BA displacement in the pHFS group measured 7.41 mm, which was significantly greater than the 4.78 mm displacement in the HC group ($p < 0.05$; Table 1).

Comparison of VA deviation rates between the HC and pHFS groups

The pHFS group had markedly higher rates of VA (89%) and BA deviation (96%) compared to the HC group (72% and 84.67%, respectively). These disparities were statistically significant ($p < 0.05$), as shown in Table 2.

Comparison of the distribution of dominant blood vessels between the HC and pHFS groups

No statistically significant differences were detected in the distribution of dominant blood vessels between the HCs and the patients in the pHFS group (Table 3).

Comparison of VA scores between the symptomatic and asymptomatic sides in the pHFS group

A statistically significant disparity in VA scores existed between the symptomatic and asymptomatic sides in the pHFS group ($p < 0.05$), suggesting a correlation

Tab. 3. Comparison of the distribution of dominant blood vessels

Dominant blood vessels	HCs 150 cases	pHFS 100 cases	Total 250 cases	CHM-x2 value	*p* value
None	88 (58.67%)	56 (56.00%)	144 (57.60%)		
Left	52 (34.67%)	31 (31.00%)	83 (33.20%)	2.7270	0.0987
Right	10 (6.67%)	13 (13.00%)	23 (9.20%)		

Tab. 4. Comparison of VA scores between symptomatic and asymptomatic sides in the pHFS group

VA score	Symptomatic side 100 cases	Asymptomatic side 100 cases	Total 200 cases	CHM-x2 value	*p* value
0	13 (13.00%)	48 (48.00%)	61 (30.50%)		
0.5	19 (19.00%)	31 (31.00%)	50 (25.00%)		
1	29 (29.00%)	15 (15.00%)	44 (22.00%)	46.731	0.0001
1.5	12 (12.00%)	0 (0.00%)	12 (6.00%)		
2	27 (27.00%)	6 (6.00%)	33 (16.50%)		

between higher VA scores on one side and an increased risk of developing HFS (Table 4).

Correlation analysis between age and VA displacement in the pHFS group

A positive correlation was demonstrated between age and VA displacement in the pHFS group, indicating that older individuals had greater VA displacement ($p = 0.034$, $r = 0.225$; Table 5).

Relationship between different sites of onset in the pHFS group and morphology of responsible blood vessels and the VBA

The variations in responsible vessels between affected sites (left vs. right) in patients with pHFS were not significantly different. The AICA and VA predominantly acted synergistically (Table 6).

DISCUSSION

C3D TOF MRA technology was used to examine the morphologic abnormalities in the VBA system among individuals with HFS and the association with pHFS. The findings revealed that pHFS patients exhibited a significantly larger diameter in the right VA, a higher displacement rate, and a greater prevalence of morphologic abnormalities in the VAs compared to the HC group.

Previous investigations, including our work (Yan *et al.* 2021), have documented anatomic deviations of VAs in HFS. The current study extended this work, as follows: (1) providing specific quantitative measurements of VA diameter asymmetries using standardized 3.0T MRA protocols; (2) examining VBA displacement patterns in a surgical population undergoing MVD; and (3) correlating morphologic parameters with demographic variables, including age. However, the fundamental observation (VBA morphologic abnormalities associated with pHFS) confirms rather than challenges existing paradigms. The clinical utility of these morphologic assessments for surgical planning or diagnostic purposes remains to be established in prospective validation studies.

Müller and Jannetta (1987) identified a distinctive electrophysiologic occurrence (termed the spread response) exclusive to individuals with HFS. This response exhibits an early wave succeeded by a delayed wave (Møller & Jannetta, 1987), highlighting the inadequacy of relying solely on MRI for HFS diagnosis because electrophysiologic assessments provide supplementary information on facial nerve functional status (Møller, 1991). While MRI has the capability

Tab. 5. Correlation analysis between age and vertebral artery displacement in the pHFS group

Diameter/Displacement	pHFS		HCs	
	r value	*p* value	r value	*p* value
Left vertebral artery diameter	-0.112	0.172	-0.023	0.781
Right vertebral artery diameter	-0.068	0.409	0.002	0.982
Vertebral artery displacement	0.225	0.034	0.029	0.763
Basilar artery diameter	-0.074	0.370	-0.013	0.875
Basilar artery displacement	0.157	0.054	0.012	0.881

Tab. 6. Variations in affected blood vessels at different sites of onset in the pHFS group

Responsible vessels	Right 49 cases	Left 51cases	Total 100 cases	*p* value
Posterior inferior cerebellar artery				0.4495
None	43 (87.76%)	42 (82.35%)	85 (85.00%)	
Found	6 (12.24%)	9 (17.65%)	15 (15.00%)	
Anterior inferior cerebellar artery				0.1265
None	3 (6.12%)	8 (15.69%)	11 (11.00%)	
Found	46 (93.88%)	43 (84.31%)	89 (89.00%)	
Superior cerebellar artery				0.3352
None	45 (91.84%)	50 (98.04%)	95 (95.00%)	
Found	4 (8.16%)	1 (1.96%)	5 (5.00%)	
Vertebral artery				0.1377
None	10 (20.41%)	5 (9.80%)	15 (15.00%)	
Found	39 (79.59%)	46 (90.20%)	85 (85.00%)	
Veins (inclusive of dykes)				1.0000
None	49 (100.00%)	50 (98.04%)	99 (99.00%)	
Found	0 (0.00%)	1 (1.96%)	1 (1.00%)	
Number of vessels				0.8185
1	9 (18.37%)	5 (9.80%)	14 (14.00%)	
2	34 (69.39%)	43 (84.31%)	77 (77.00%)	
3	6 (12.24%)	3 (5.88%)	9 (9.00%)	

to visualize vascular loops associated with the onset of HFS, some HFS cases may exhibit morphologic changes in the VBA system without concurrent clinical symptoms (Møller & Jannetta, 1987; Møller, 1991).

VBA stenosis can reduce the space within the posterior cranial fossa, potentially increasing the risk of compression on the facial nerve. Studies have demonstrated a significant association between the direction of VA artery displacement and the side of HFS symptoms (Pico *et al.* 2015; Battistelli *et al.* 2024). The findings revealed that pHFS patients exhibited a significantly larger diameter in the right VA, a higher displacement rate, and a greater prevalence of morphologic abnormalities in the VAs compared to the HC group. The results herein are consistent with the extant literature. Factors, such as BA elongation and dilation, may be attributed to decreased medial elastic tissue and ruptured internal elastic lamina, which are commonly linked to vascular risk factors, like age, gender, and hypertension (Pico *et al.* 2015).

While several morphologic parameters demonstrated statistical significance, the clinical relevance of the observed differences warrants consideration. For example, the right VA diameter difference of 0.24 mm between the pHFS and HC groups (2.71 mm vs. 2.47 mm, respectively; $p < 0.05$) represents a 9.7% change. Whether such differences meaningfully influence neurovascular compression (NVC) mechanics or surgical decision-making requires biomechanical modeling or prospective correlation with surgical outcomes. The precision of measurement (0.01 mm) exceeds the spatial resolution of clinical MRA and measurement error may approach the magnitude of reported differences.

Moreover, the association between VBA morphologic abnormalities and pHFS does not establish causation. Three scenarios merit consideration: (1) morphologic abnormalities predispose to neurovascular compression triggering pHFS (causal); (2) pHFS-related vascular pulsation induces secondary morphologic remodeling (reverse causation); or (3) shared underlying factors (e.g., connective tissue properties and vascular wall composition) independently influence morphology and compression susceptibility (confounding). Longitudinal studies tracking morphologic changes over disease course combined with biomechanical modeling of compression dynamics are needed to elucidate pathophysiologic mechanisms. A critical observation was that morphologic VBA abnormalities occurred in asymptomatic individuals, indicating that anatomic variation alone is insufficient to cause pHFS. This finding suggests a 'multiple-hit' model in which morphologic predisposition requires additional factors (possibly neurovascular contact location, pulsatile dynamics, nerve vulnerability, or inflammatory susceptibility) to manifest clinically. Understanding why some individuals with morphologic risk remain asymptomatic represents a key frontier for preventive strategies.

CT imaging exhibits restricted sensitivity for diagnosing the underlying cause of HFS, primarily detecting significant regions of subacute and chronic infarction, intracranial tumors, intracranial hemorrhage, or extensive meningeal abnormalities (Xiang *et al.* 2024; Yang, 2024). CT remains an essential consideration for cases in which MRI is not feasible. High-resolution 3D MRI has demonstrated high accuracy in preoperative pHFS and sHFS assessment (Wang *et al.* 2024). Despite proficiency in delineating neurovascular relationships, MRI may not offer insights into nerve excitability or predict symptom progression in cases of NVC before the onset of HFS symptoms. This limitation underscores the need to use multi-modal assessments in intricate HFS cases. The 3D TOF spoiled gradient-recalled acquisition MRA technique is commonly used to visualize abnormal blood vessels, combining inflow enhancement and saturation effects to delineate the facial nerve proximity to neighboring vessels (Cui & Ling, 2015). T1-weighted imaging is well-suited for highlighting neural anatomic structures, displaying moderate signal intensity along the facial nerve pathway distinct from the high signal intensity of surrounding vessels. Utilizing 3D high-resolution acquisition prevents image blurring and aids in tracking intracranial arteries and the branches. This sequence demonstrates reduced sensitivity to slow venous flow, necessitating thorough scanning in cases of suspected venous compression. Integration of magnetic resonance cisternography with 3D TOF MRA image fusion enhances the illustration of neurovascular relationships in HFS patients (Satoh *et al.* 2007). The 3D contrast-enhanced T1-weighted imaging sequence is valuable for assessing pHFS using the MRA method, particularly in excluding sHFS due to tumors, inflammation, vascular abnormalities, or demyelinating diseases (Campos-Benitez & Kaufmann, 2008; Hyun *et al.* 2010).

Taken together, MRI, a non-invasive imaging technique, offers significant advantages in delineating responsible vessels. High-resolution MRI scans and MRA are currently preferred for diagnosing and managing HFS patients. This preference underscores the rationale for choosing MRI as the primary imaging modality in the current study.

NVC at the REZ of the facial nerve is believed to induce demyelination, causing abnormal nerve impulse conduction and contributing significantly to the pathogenesis of HFS (Prasad & Galetta, 2009). However, there is ongoing confusion regarding the precise anatomic definition of the REZ, often leading to its incorrect identification with the transitional zone [TZ] (Obersteiner Redlich zone). Unlike the TZ, which acts as a transition between central and peripheral myelin, the REZ refers explicitly to the area where the facial nerve diverges from the brainstem and begins to interact with blood vessels (Quanchareonsap *et al.* 2023). Recent studies (Tomii *et al.* 2003; Prasad & Galetta, 2009) have proposed a classification of the facial nerve REZ into the following four distinct segments, followed by the facial nerve cisternal segment where myelin phospholipids are exclusively provided by Schwann cells: the root exit point (RExP); the adherent segment (AS); the root detachment point (RDP); and the TZ. Axial MRI images may not effectively distinguish between the anterior and posterior segments of the REZ due to the facial nerve proximity to the brainstem. Conversely, oblique coronal reformat images offer the best perspective for visualizing the entire trajectory of the facial nerve REZ, illustrating the transition from the anterior segment to the REZ and RDP (Donahue *et al.* 2017). The pathophysiologic mechanisms underlying pHFS are not fully elucidated but compression of the facial nerve by blood vessels is a key factor in increased excitability. High-resolution MRI scans and MRA have emerged as the preferred imaging modalities for diagnosing and treating HFS patients (Tomii *et al.* 2003; Prasad & Galetta, 2009; Quanchareonsap *et al.* 2023; Hou *et al.* 2024; Duvvuri *et al.* 2025), justifying the correct selection for this study.

An important consideration is the age disparity between groups. Given the significant positive correlation between age and VA displacement (p = 0.034, r = 0.225), the observed morphologic differences may partially reflect age-related vascular changes rather than pHFS-specific pathology. Future studies should use age-matched controls or age-adjusted statistical analyses to isolate disease-specific effects from age-related vascular remodeling. In addition, the study population consisted exclusively of pHFS patients undergoing microvascular decompression surgery, representing a selected subset with severe, medication-refractory symptoms. This finding introduces selection bias because patients with milder disease or patients responding to medical management were excluded. Consequently, observed morphologic abnormalities may correlate with disease severity rather than pHFS per se. Generalization to non-surgical pHFS populations or early-stage disease requires validation in broader, community-based cohorts.

Limitations

This study had several limitations. First, as a single-institution retrospective study from a tertiary referral center, findings may not generalize to other populations due to referral bias, institutional imaging protocols, and surgical expertise variations. The relatively small proportion of unilateral VA migration across the midline, so the missing value is large, which contributes to bias of the data. Multi-center prospective validation is needed before widespread clinical application. Second, although 3.0 T MRA imaging was chosen for detailed visualization of vascular structures, variations in imaging quality and potential operator-dependent measurement discrepancies could affect the accuracy of anatomic assessments, such as VA displacement and vessel diameter. Third, the reliance on cross-sectional

imaging data limited the ability to infer longitudinal changes in vascular morphology or establish a causal relationship with HFS progression. Fourth, the study did not comprehensively address potential confounding factors, such as genetic predispositions or lifestyle influences, which could impact vascular characteristics and HFS incidence. Fifth, the substantial missing data for VA displacement measurements (64% in the pHFS group and 67.3% in the HC group) significantly limited the validity of these findings. Missing data resulted from the retrospective nature of this study and the poor image quality of the reviewed cases. Results regarding displacement should be interpreted with extreme caution and require validation in prospective studies with complete data capture. Sixth, multiple statistical comparisons were performed without correction for family-wise error rate (e.g., Bonferroni adjustment). This statistical method increases the risk of type I errors and findings should be interpreted accordingly. Applying a conservative Bonferroni correction ($\alpha = 0.05$/k comparisons) would require a $p < 0.005$ for significance, which some of the study findings may not meet. Replication in independent cohorts is essential. Seventh, inter-rater reliability assessment was not systematically performed, representing a limitation in measurement validity. Future studies should incorporate formal reliability testing with an intraclass correlation coefficient (ICC) > 0.80 as a quality threshold. Finally, the VA scoring system was adapted from a Xi'an Jiaotong University protocol without independent validation in our population. The weighting scheme (0, 0.5, 1, 1.5, and 2 points) reflects anatomic displacement severity but lacks empirical validation against clinical outcomes or surgical findings in our cohort. Validation of this scoring system through correlation with intraoperative findings would strengthen future applications. Future prospective studies with larger, more diverse cohorts and advanced imaging techniques are imperative to better understand the pathophysiology of HFS and confirm the identified associations. Finally, because this study was conducted in a specialized clinical setting, the MVD outcomes may not directly apply to centers with varying expertise or resources.

CONCLUSION

This study utilized 3D TOF MRA technology to determine the relationship between morphologic abnormalities in the VAs and BAs and pHFS. The results revealed that pHFS patients exhibited significantly larger diameters and displacements in these arteries compared to the HC group. Moreover, the displacement rates were notably higher in the pHFS cohort. Furthermore, distinct variances in arterial morphologic features were observed between the symptomatic and asymptomatic sides in patients with HFS, indicating a strong link between arterial morphologic changes and the development of HFS.

FUNDING

This research did not receive any specific grant from funding agencies in the public, commercial, or not-for-profit sectors.

CONSENT FOR PUBLICATION

Not applicable.

AVAILABILITY OF DATA AND MATERIALS

The datasets are available from the corresponding author on reasonable request.

AUTHOR CONTRIBUTIONS

Conceptualization: Hao Zhang, Jinming Yan
Investigation: Hao Zhang, Jinming Yan
Formal Analysis: Hao Zhang, Jinming Yan
Data Curation: Hao Zhang, Jinming Yan
Supervision: Hao Zhang
Writing - Original Draft: Hao Zhang, Jinming Yan
Writing - Review & Editing: Hao Zhang, Jinming Yan

ACKNOWLEDGMENTS

Not applicable.

REFERENCES

1 Aktan D, Depierreux F. How to face the hemifacial spasm: challenges and misconceptions. Acta Neurologica Belgica. 2024; **124**(1): 17–23.
2 Battistelli M, Izzo A, D'Ercole M, D'Alessandris QG, Di Domenico M, Ioannoni E, et al. Optimizing surgical technique in microvascular decompression for hemifacial spasm–Results from a surgical series with contemporary use of neuronavigation and intraoperative neuromonitoring. Surgical Neurology International. 2024; **15**: 319.
3 Błaszczyk M, Ochwat K, Necka S, Kwiecińska M, Ostrowski P, Bonczar M, et al. The Arterial Anatomy of the Cerebellum—A Comprehensive Review. Brain Sciences. 2024; **14**(8): 763.
4 Campos-Benitez M, Kaufmann AM. Neurovascular compression findings in hemifacial spasm. Journal of neurosurgery. 2008; **109**(3):416-20.
5 Colosimo C, Bologna M, Lamberti S, Avanzino L, Marinelli L, Fabbrini G, et al. A comparative study of primary and secondary hemifacial spasm. Archives of Neurology. 2006; **63**(3): 441–4.
6 Cui Z, Ling Z. Advances in microvascular decompression for hemifacial spasm. Journal of Otology. 2015; **10**(1): 1–6.
7 Donahue JH, Ornan DA, Mukherjee S. Imaging of vascular compression syndromes. Radiologic Clinics. 2017; **55**(1): 123–38.
8 Dou N-N, Zhong J, Liu M-X, Xia L, Sun H, Li B, et al. Management of bilateral hemifacial spasm with microvascular decompression. World Neurosurgery. 2016; **87**: 640–5.
9 Duvvuri M, Ali H, Amans MR. Non-invasive imaging modalities for diagnosing pulsatile tinnitus: a comprehensive review and recommended imaging algorithm. J Neurointerv Surg. 2025 Jan 25:jnis-2023-020949.
10 Fang J, Lv G, Wang D, Liu R. The Distance Between the Cranial Nerve IX-X Root Entry/Exit Zone and the Pontomedullary Sulcus: MR Imaging Study in Patients With Hemifacial Spasm. Frontiers in Neurology. 2022; **13**: 819488.

11 Hou X, Xu Rx, Tang J, Yin C. A novel 3D multimodal fusion imaging surgical guidance in microvascular decompression for primary trigeminal neuralgia and hemifacial spasm. Head & Face Medicine. 2024; **20**(1): 56.
12 Hyun S-J, Kong D-S, Park K. Microvascular decompression for treating hemifacial spasm: lessons learned from a prospective study of 1,174 operations. Neurosurgical review. 2010; **33**: 325–34.
13 Joo B-E. Research on the Pathogenesis of Hemifacial Spasm through Electrophysiological Studies. Journal of Electrodiagnosis and Neuromuscular Diseases. 2023; **25**(3): 105–10.
14 Møller AR. Interaction between the blink reflex and the abnormal muscle response in patients with hemifacial spasm: results of intraoperative recordings. Journal of the neurological sciences. 1991; **101**(1): 114–23.
15 Møller AR, Jannetta PJ. Monitoring facial EMG responses during microvascular decompression operations for hemifacial spasm. Journal of neurosurgery. 1987; **66**(5): 681–5.
16 Nurminen P, Marjamaa J, Niemelä M, Sairanen T. Incidence and prevalence of Hemifacial Spasm in Finland's largest hospital district. Journal of the Neurological Sciences. 2023; **446**: 120587.
17 Perren F, Magistris MR. Is hemifacial spasm accompanied by hemodynamic changes detectable by ultrasound? Acta neurochirurgica. 2014; **156**: 1557–60.
18 Pico F, Labreuche J, Amarenco P. Pathophysiology, presentation, prognosis, and management of intracranial arterial dolichoectasia. The Lancet Neurology. 2015; **14**(8): 833–45.
19 Prasad S, Galetta S. Trigeminal neuralgia: historical notes and current concepts. The neurologist. 2009; **15**(2): 87–94.
20 Quanchareonsap W, Jariyakosol S, Apinyawasisuk S, Roumwong A, Chentanez V. Microanatomy of the central myelin portion and transitional zone of the oculomotor and abducens nerves. Folia Morphologica. 2023; **82**(3): 543–50.
21 Satoh T, Onoda K, Date I. Fusion imaging of three-dimensional magnetic resonance cisternograms and angiograms for the assessment of microvascular decompression in patients with hemifacial spasms. Journal of neurosurgery. 2007; **106**(1): 82–9.
22 Tomii M, Onoue H, Yasue M, Tokudome S, Abe T. Microscopic measurement of the facial nerve root exit zone from central glial myelin to peripheral Schwann cell myelin. Journal of neurosurgery. 2003; **99**(1): 121–4.
23 Truong VT, Ngo MQ, Phan D, Le H, Hoang NAT. Results from 228 Patients with Hemifacial Spasm Undergoing Microvascular Decompression without Intraoperative Neuroelectrophysiology Monitoring. World Neurosurgery. 2024; **185**: e461–e6.
24 Wang B, Wei X, Qi H, Bao X, Hu M, Ma J. Efficacy and safety of botulinum neurotoxin in the treatment of hemifacial spasms: a systematic review and meta-analysis. BMC neurology. 2024; **24**(1): 420.
25 Wang L, Hu X, Dong H, Wang W, Huang Y, Jin L, Luo Y, Zhang W, Lian Y, Liang Z, Shang H, Feng Y, Wu Y, Chen J, Luo W, Wan X. Clinical features and treatment status of hemifacial spasm in China. Chin Med J (Engl). 2014; **127**(5): 845–9.
26 Wang Y, Li Y, Shi H, Du Y, Guo W, Shi H, et al. The value of multimodal imaging fusion in preoperative visualization assessment of neurovascular relationship in hemifacial spasm: a single-center retrospective study. Neurosurgical Review. 2024; **47**(1): 605.
27 Xiang G, Sui M, Jiang N, Luo R, Xia J, Wei X, et al. The progress in epidemiological, diagnosis and treatment of primary hemifacial spasm. Heliyon. 2024; **10**(19).
28 Yang M. Ruptured aneurysm at the meatal loop of the posterior inferior cerebellar artery: a case description. Quantitative Imaging in Medicine and Surgery. 2024; **14**(6): 4232.
29 Yan X, Gu J, Quan J, Zhang X, Zhou X, Qu J, et al. Anatomical deviations of vertebral artery in hemifacial spasm: a quantitative study. Surgical and Radiologic Anatomy. 2021; **43**: 291–9.
30 Zhou J, Zhan Y, Xie Y, Deng B, Yuan S, Jiang L, et al. MRI measurements the linear volume of posterior cranial fossa in patients with hemifacial spasm. Journal of Clinical Neuroscience. 2022; **101**: 94–9.